N-to-sRGB Mapping for Single-Sensor Multispectral Imaging

Yusuke Monno, Masayuki Tanaka, and Masatoshi Okutomi
Department of Mechanical and Control Engineering
Tokyo Institute of Technology

Abstract

Visualization of a multispectral image in a standard color space, typically the sRGB space, is an important task for human color perception. When we reproduce the sRGB image from the multispectral image with N spectral bands, an N-to-sRGB mapping is required. The challenge of the N-to-sRGB mapping in single-sensor multispectral imaging with a multispectral filter array (MSFA) is to reduce demosaicking error amplification and propagation across different spectral bands, which are not trivial because of very sparse sampling of multiple spectral bands in a single image sensor. In this paper, we propose a novel N-to-sRGB mapping pipeline for effectively suppressing the demosaicking error amplification and propagation. Our idea is to apply guided filtering in the mapped sRGB space using one of input N band images before the amplification and propagation as a guide image. Experimental results demonstrate that our proposed pipeline improves the mapping accuracy for various MSFA types.

1. Introduction

In recent years, single-sensor multispectral imaging with a multispectral filter array (MSFA) has received increasing attention for practical one-shot multispectral image acquisition [15]. In the MSFA, more than three spectral bands are arrayed. Figure 1 (a) shows an example of the MSFA, which aims at simultaneous capturing of visible and near-infrared (NIR) images [3, 20, 30].

In multispectral imaging, a main purpose is to acquire an associated multispectral image. However, accurate visualization of the multispectral image in a standard color space is still important for human color perception. Let us consider an example of the RGB-NIR filter array in Fig. 1 (a). Figure 1 (b) shows the spectral sensitivities of typical R, G, B, and NIR filters. Since the typical R, G, and B filters have sensitivities also in NIR wavelengths[1], the color of the acquired RGB image (Fig. 1 (c)) significantly differs from human color perception. Therefore, a mapping[2] from the sensor multispectral space to a standard color space, typically the display sRGB space (Fig. 1 (d)), is required.

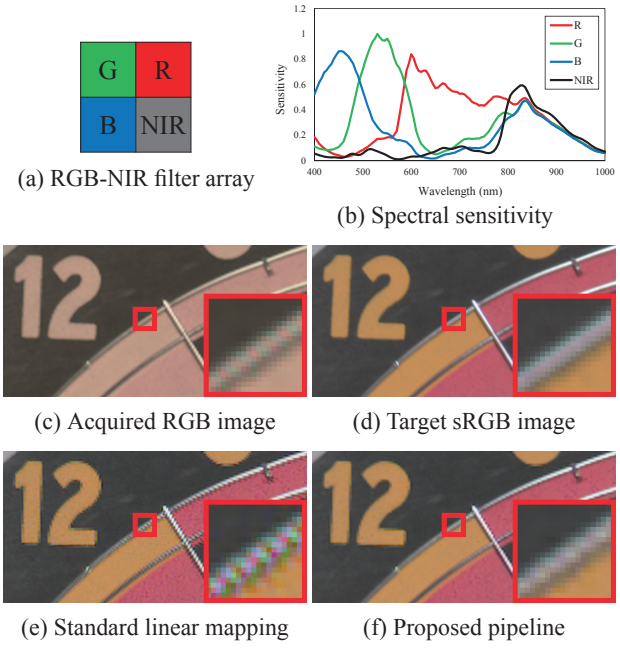

(a) RGB-NIR filter array (b) Spectral sensitivity

(c) Acquired RGB image (d) Target sRGB image

(e) Standard linear mapping (f) Proposed pipeline

Figure 1. Single-sensor RGB-NIR imaging. (a) The RGB-NIR filter array proposed in [3, 20, 30], (b) the spectral sensitivities of the filters, (c) the acquired RGB image by bicubic interpolation, (d) the ground-truth target sRGB image, (e) the result of a standard linear mapping, and (f) the result of our proposed pipeline.

Figure 2 shows a standard imaging pipeline of the single-sensor multispectral imaging. Generally speaking, in the single-sensor multispectral imaging with N spectral bands, only one pixel value among N-band values is recorded at each pixel location. This sensor output is called raw MSFA data. Then, a full multispectral image is reconstructed from the raw MSFA data by an interpolation process called multispectral demosaicking [18, 22, 24]. The interpolated multispectral image is used for acquiring associated multispectral

[1] In standard color imaging, an NIR-cut filter is placed in front of the image sensor to avoid NIR contaminations of the captured RGB image.

[2] In this context, it is also called color correction.

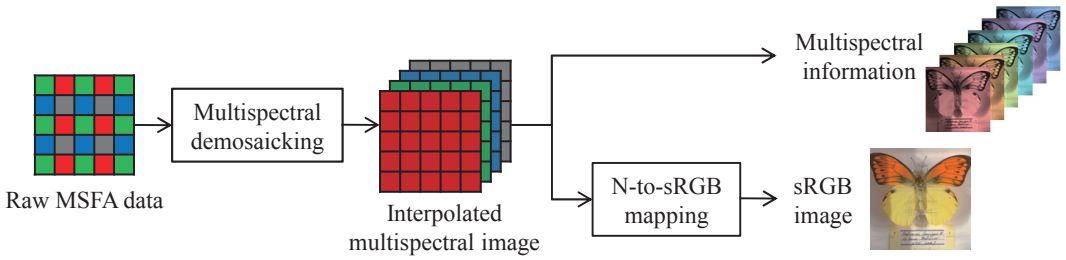

Figure 2. A standard single-sensor multispectral imaging pipeline.

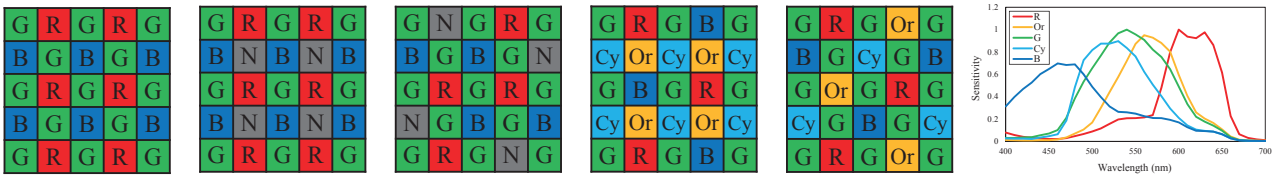

(a) Bayer RGB (b) Uniform RGB-NIR (c) Hybrid RGB-NIR (d) Miao and Qi five band (e) Monno et al. five band (f) Spectral sensitivities of the five-band filters

Figure 3. Various MSFA types. (a) The Bayer CFA [1] as a reference, (b) the uniform RGB-NIR filter array [3, 20, 30], (c) the hybrid RGB-NIR filter array [14], (d) the five-band filter array proposed by Miao and Qi [21], (e) the five-band filter array proposed by Monno et al. [25], and (f) the spectral sensitivities of the five-band filters in [24], which are called R, Or, G, Cy, and B band, respectively.

information or mapped to the display sRGB space[3] for color visualization. We generally use the term "*N-to-sRGB mapping*" in describing the mapping from a multispectral sensor space with N spectral bands to the sRGB color space.

The challenge of the N-to-sRGB mapping in the single-sensor multispectral imaging is to reduce demosaicking error amplification and propagation across different spectral bands, which are not trivial due to an increased number of arrayed spectral bands in the MSFA from the standard Bayer color filter array (CFA) [1], as shown in Fig. 3 (a)-(e). Figure 1 (e) shows an example result of the N-to-sRGB mapping by a standard linear mapping [11]. One can see that the demosaicking artifacts in the input RGB image (Fig. 1 (c)) are severely amplified in Fig. 1 (e). To the best of our knowledge, none of existing algorithms address the demosaicking errors in the N-to-sRGB mapping.

In this paper, we propose a novel N-to-sRGB mapping pipeline for effectively reducing the demosaicking error amplification and propagation. Our idea is to apply guided filtering [8] in the mapped sRGB space using one of input N band images before the amplification and propagation as a guide image. We analytically show that the error amplification and propagation can be filtered out by the guided filtering if we can obtain an effective guide image with small errors. In experiments, we demonstrate that our proposed pipeline improves the mapping accuracy for various MSFA types compared with existing algorithms. Figure 1 (f) shows an example result of our proposed mapping pipeline. One can see that the guided filtering process effectively suppresses the demosaicking artifacts in Fig. 1 (f).

[3]We discuss the mapping to the sRGB space in this paper. However, our proposed pipeline in Sec. 5 is not limited to this.

2. Single-Sensor Multispectral Imaging

In this section, we briefly review existing works related to the single-sensor multispectral imaging pipeline in Fig. 2.

2.1. MSFAs and Demosaicking Algorithms

One category of the MSFAs, which is typically called an RGB-NIR filter array, is designed for simultaneous acquisition of visible and NIR images. The authors of [17, 29] respectively proposed an optimized filter array by describing a whole imaging pipeline in a linear form. In [3, 20, 30], the authors realized the development of prototype RGB-NIR cameras with the uniform RGB-NIR filter array shown in Fig. 3 (b). In [14], Kiku et al. proposed the hybrid color filter array (CFA) as shown in Fig. 3 (c). To preserve the quality of the acquired RGB image, the hybrid CFA keeps the sampling density of the G band as high as the Bayer CFA (Fig. 3 (a)) [1], which is the most widely used CFA in current color digital cameras.

Another category is an MSFA with more than three spectral bands in visible wavelengths mainly for acquiring accurate spectral information. In [21], Miao and Qi proposed a generic method for designing an MSFA with given number of spectral bands. Figure 3 (d) shows an example five-band filter array generated by the generic method. In [25], Monno et al. proposed a five-band filter array with the advantage of the high sampling density of the G band as shown in Fig. 3 (e). In [24], they also developed a prototype five-

band camera with the spectral sensitivities in Fig. 3 (f). A uniform six-band filter array [2] and a seven-band assorted pixel mosaic [31] have also been proposed.

In conjunction with the development of the various MSFAs, multispectral demosaicking algorithms have also been proposed. Existing algorithms include edge-sensing interpolation [22], color difference interpolation [2, 20], linear demosaicking [17, 29, 31], and guided filtering based interpolation [14, 23, 24]. However, their performance is still imperfect because of the difficulty of the multispectral demosaicking due to very sparse sampling of each spectral band in the MSFA. This paper addresses non-trivial demosaicking errors in the N-to-sRGB mapping. We finally refer a recent paper [15] for comprehensive reviews in this field.

2.2. N-to-sRGB Mapping Algorithms

The N-to-sRGB mapping is closely related with color correction algorithms, which map color camera's RGB responses to a standard color space [11]. Many algorithms have been proposed for the color correction. Representative algorithms include least-square linear [11] and polynomial mappings [9], color correction in the DCT domain [13], use of look-up tables [10], and a neural network approach [12]. Because of their simplicity, the linear and polynomial mappings are widely used in digital image processing pipelines. Finlayson et al. recently proposed a root-polynomial mapping [5], which modifies the polynomial mapping by taking k^{th} root of each k-degree term to improve the robustness in intensity changes. All of these mapping algorithms can straightforwardly be extended for the N-to-sRGB mapping by increasing the dimensionality of the input data [3].

In multispectral imaging, the sRGB image is often reproduced by a spectral estimation based approach with a linear spectral model [19, 28], which first estimates the spectral distributions of the captured scene and then renders those distributions to the sRGB space. This approach can also be interpreted as the N-to-sRGB mapping by rewriting resultant mathematical expressions. In the context of a multispectral-to-color mapping, image fusion based algorithms have also been proposed [4, 16]. However, the purpose of these works is image enhancement, which is different from accurate color visualization in the sRGB space handled in this paper. Our proposed pipeline described in Sec. 5 is independent of the mapping algorithms and can generally incorporate any existing mapping algorithms.

Recently, an image restoration approach [30], which jointly handles the demosaicking and the mapping, has also been proposed and shown superior performance at the cost of high computational cost.

3. N-to-sRGB Mapping Formulation

In this section, we extend the linear [11], polynomial [9] and root-polynomial [5] mappings for the N-to-sRGB mapping. We use these mappings because of their simplicity.

The N-to-sRGB mapping is generally described as

$$\mathbf{q} = \mathbf{M}\mathbf{p}, \tag{1}$$

where $\mathbf{q} = [r^s, g^s, b^s]^T$ is a target sRGB vector, $\mathbf{M}$ is a mapping matrix, and $\mathbf{p}$ is a input intensity vector. The superscript s represents the values in the sRGB space. Let us consider a case of the RGB-NIR imaging and a linear mapping from R, G, B, and NIR responses to the sRGB values. The linear mapping is specifically described as

$$\begin{bmatrix} r^s \\ g^s \\ b^s \end{bmatrix} = \begin{bmatrix} m_{11} & m_{12} & m_{13} & m_{14} \\ m_{21} & m_{22} & m_{23} & m_{24} \\ m_{31} & m_{32} & m_{33} & m_{34} \end{bmatrix} \begin{bmatrix} r \\ g \\ b \\ n \end{bmatrix}, \tag{2}$$

where $\mathbf{p} = [r, g, b, n]^T$ is a input intensity vector and n represents the intensity of the NIR band.

The matrix $\mathbf{M}$ is calculated from training samples by least-square regression as

$$\mathbf{M} = \mathbf{Q}\mathbf{P}^T(\mathbf{P}\mathbf{P}^T)^{-1}, \tag{3}$$

where $\mathbf{Q}$ is a $3 \times K$ matrix containing target sRGB vectors of K training samples, and $\mathbf{P}$ is a $4 \times K$ matrix containing corresponding input four-dimensional vectors of K training samples.

The polynomial and the root-polynomial mappings are similarly expressed. For example, the input vector of the second-order polynomial mapping with an offset term is described as

$$\mathbf{p} = [r, g, b, n, r^2, g^2, b^2, n^2, rg, rb, rn, gb, gn, bn, 1]^T, \tag{4}$$

and the input vector of the corresponding root-polynomial mapping is describes as

$$\mathbf{p} = [r, g, b, n, \sqrt{rg}, \sqrt{rb}, \sqrt{rn}, \sqrt{gb}, \sqrt{gn}, \sqrt{bn}, 1]^T. \tag{5}$$

Note that the dimension of the root-polynomial mapping decreases because $[\sqrt{r^2}, \sqrt{g^2}, \sqrt{b^2}, \sqrt{n^2}]^T = [r, g, b, n]^T$.

4. Demosaicking Error Amplification and Propagation

In this section, we analyze the demosaicking error amplification and propagation across spectral bands. Let us consider the N-to-sRGB mapping described in Eq. (1). The mapping with demosaicking errors is described as

$$\mathbf{q} = \mathbf{M}\begin{bmatrix} r + e_r \\ g + e_g \\ b + e_b \\ n + e_n \end{bmatrix} = \mathbf{M}\begin{bmatrix} r \\ g \\ b \\ n \end{bmatrix} + \mathbf{M}\begin{bmatrix} e_r \\ e_g \\ e_b \\ e_n \end{bmatrix}, \tag{6}$$

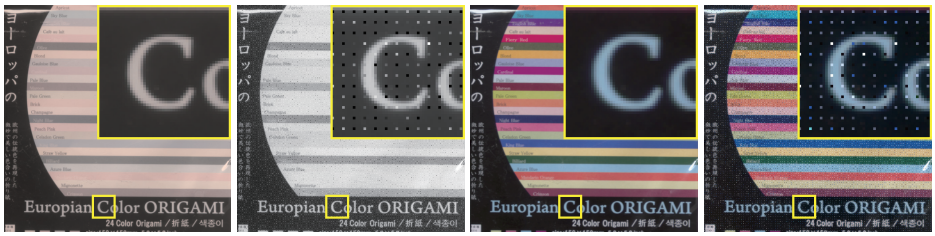

(a) Input RGB without errors (b) Input NIR with errors (c) Target ground-truth sRGB (d) Mapped sRGB

Figure 4. Propagation of demosaicking errors across spectral bands. (a) The input RGB without the demosaicking errors, (b) the input NIR with the demosaicking errors, (c) the target ground-truth sRGB, and (d) the mapped sRGB by the linear mapping.

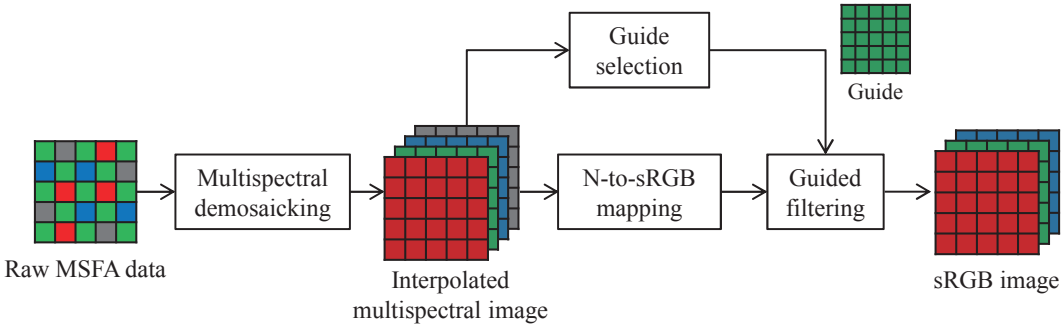

Figure 5. Proposed N-to-sRGB mapping pipeline for the single-sensor multispectral imaging.

where $[e_r, e_g, e_b, e_n]^T$ is a vector representing the demosaicking errors.

The amplification of the demosaicking errors occurs when the matrix norm of $\mathbf{M}$ is larger than one as

$$||\mathbf{M}||_2 = \max_{\mathbf{p}\neq\mathbf{0}} \frac{||\mathbf{M}\mathbf{p}||_2}{||\mathbf{p}||_2} > 1, \tag{7}$$

which is often the case in the RGB-NIR imaging when the illumination has large spectral powers in NIR wavelengths.

To explain the demosaicking error propagation, let us consider a simple example that the demosaicking error is included only in the NIR band as

$$\mathbf{q} = \mathbf{M}\begin{bmatrix} r \\ g \\ b \\ n \end{bmatrix} + \mathbf{M}\begin{bmatrix} 0 \\ 0 \\ 0 \\ e_n \end{bmatrix}. \tag{8}$$

If we assume the linear mapping described in Eq. (2), Eq. (8) is rewritten as

$$\mathbf{q} = \mathbf{q}_0 + \begin{bmatrix} m_{14} \\ m_{24} \\ m_{34} \end{bmatrix} e_n, \tag{9}$$

where $\mathbf{q}_0$ represents the mapped sRGB vector without the demosaicking errors. In Eq. (9), it is obvious that the error in the NIR band are propagated into the mapped sRGB values when the coefficients of the NIR term, i.e., m_{14}, m_{24}, and m_{34} have non-zero values.

Figure 4 visually explains the demosaicking error propagation. Figure 4 (a) and (b) are simulated images under an incandescence light, assuming only the NIR band contains demosaicking errors. The demosaicking errors are simulated by random errors of a regular grid pattern in Fig. 4 (b). Figure 4 (c) and (d) show the target ground-truth sRGB image and the mapped sRGB image, respectively. One can see that the regular errors are severely propagated in Fig. 4 (d).

5. Proposed N-to-sRGB Mapping Pipeline

Figure 5 shows our proposed N-to-sRGB mapping pipeline for reducing the demosaicking error amplification and propagation in the single-sensor multispectral imaging. Our idea is to apply the guided filtering [8] in the mapped sRGB space using one of input N band images before the amplification and propagation as a guide image. The guided filtering is a powerful edge-preserving filtering algorithm [8]. The output of the guided filtering is expressed as a linear transformation of a given guide image, which preserves the image structures of the guide image. In the following, the filtering process for the R band in the mapped sRGB image is explained. The G band and the B band are similarly processed.

At a local image window, the output of the guided filtering is described by a linear transformation of a given guide image as

$$f_k = \alpha I_k + \beta, \quad \forall k \in \omega, \tag{10}$$

where ω denotes the local image window, k represents a pixel location in the window, f_k is the filtering output, and I_k is the intensity of the guide image. The linear coefficients (α, β) are determined as

$$(\alpha, \beta) = \min_{\alpha,\beta} \sum_{k\in\omega} \left(r_k^s - (\alpha I_k + \beta)\right)^2, \tag{11}$$

where r_k^s is the intensity of the filtering input, i.e., the R value of the mapped sRGB image[4]. The overlaps of the local windows are uniformly or weighted averaged.

We analytically show that the error amplification and propagation can be filtered out by the guided filtering under the following assumptions: (i) each band image can be approximated by the linear transformation of the guide image, (ii) the guide image contains relatively small errors, and (iii) the demosaicking error is a random variable with zero mean. The proposed pipeline selects the guide image from the interpolated N band images before the mapping. Since the quality of the guide image plays a crucial role, the spectral band with minimum demosaicking errors is selected for the guide image. For example, recent progress on the MSFA design [14, 24] has shown that the MSFAs with the high sampling density of the G band, such as Fig. 3 (c) and (e), can generate high-quality guide images. For these MSFAs, the G-band image is selected for the guide image.

Let us consider the linear mapping in Eq. (6) again. The first row of Eq. (6) is expanded as

$$\begin{aligned} r^s = {} & m_{11}(r + e_r) + m_{12}(g + e_g) \\ & + m_{13}(b + e_b) + m_{14}(n + e_n). \end{aligned} \tag{12}$$

Suppose the G band is selected for the guide image and the guide image ideally contains no error, i.e., $g + e_g = g = I$, where I represents the guide. Based on the assumption (i), the underlying each band value is expressed as

$$\begin{aligned} r &\simeq \alpha_r I + \beta_r, \quad g = I, \\ b &\simeq \alpha_b I + \beta_b, \quad n \simeq \alpha_n I + \beta_n, \end{aligned} \tag{13}$$

where (α_r, β_r), (α_b, β_b), and (α_n, β_n) are linear coefficients for the R, B, and NIR bands, respectively.

Equation (12) is rewritten by substituting Eq. (13) as

$$\begin{aligned} r^s &\simeq m_{11}(\alpha_r I + \beta_r + e_r) + m_{12} I \\ &\quad + m_{13}(\alpha_b I + \beta_b + e_b) + m_{14}(\alpha_n I + \beta_n + e_n) \\ &\simeq \alpha' I + \beta' + X^e, \end{aligned} \tag{14}$$

where $\alpha' = m_{11}\alpha_r + m_{12} + m_{13}\alpha_b + m_{14}\alpha_n$, $\beta' = m_{11}\beta_r + m_{13}\beta_b + m_{14}\beta_n$, and $X^e = m_{11}e_r + m_{13}e_b + m_{14}e_n$.

[4]The original guided filtering also has a regularization term, which constrains the smoothness of the output image [8]. We omit the regularization term for the analysis in this section. Actually, we used a very small regularization weight in experiments.

Based on Eq. (14), Eq. (11) is rewritten as

$$(\alpha, \beta) = \min_{\alpha,\beta} \sum_{k\in\omega} \left(\alpha' I_k + \beta' + X_k^e - (\alpha I_k + \beta)\right)^2. \tag{15}$$

In Eq. (15), if we assume that the demosaicking error is a random variable with zero mean, the expected value of X^e equals zero, i.e., $E[X^e] = 0$, and the solution of Eq. (15) reduces $(\alpha, \beta) \simeq (\alpha', \beta')$. Therefore, the output of the filtering is expressed as

$$f_k = \alpha' I_k + \beta', \quad \forall k \in \omega. \tag{16}$$

Equation (16) shows that if the demosaicking errors in the guide image are small, the term X^e, which represents the error amplification and propagation, is filtered out by the guided filtering.

6. Experiments

6.1. Experimental Setups

Dataset and Illumination. We captured a new hyperspectral image dataset including both visible and NIR wavelengths (420-1000nm). The hyperspectral image is acquired at every 10 nm by using a monochrome camera with two VariSpec tunable filters [7], VIS (420-640nm) and SNIR (650-1000nm). The captured hyperspectral image is then converted into a form of spectral reflectance using a calibration chart. In experiments, the whole imaging pipeline is simulated by using the hyperspectral dataset as the ground truth. The dataset consists of 40 scenes with 512×512 pixels, which is divided into two groups, where half 20 scenes are used for training mapping matrices and the rest 20 scenes are used for testing the proposed pipeline. We consider five illuminations; an incandescent light, a diva light (a professional fluorescent light), an LED light, a fluorescent light, and the daylight.

MSFAs and demosaicking algorithms. Our proposed pipeline is tested for four MSFA types shown in Fig. 3. For each MSFA, state-of-the-art demosaicking algorithm is used as follows: (i) the algorithm [20] is used for the uniform RGB-NIR filter array, (ii) the algorithm [14] is used for the hybrid RGB-NIR filter array, (iii) the algorithm [26] is used for the five-band filter array by Miao and Qi, and (iv) the algorithm [23] is used for the five-band filter array by Monno et al.

Mapping algorithms. Linear [11], polynomial [9], and root-polynomial [5] mappings are used as described in Sec. 3. The second order with the offset term is also used in the polynomial and the root-polynomial mappings for the five-band filter arrays. To simplify the problems, we assume that the illumination condition is known and the mapping matrix is calculated for each illumination. Note that

Table 1. Comparison of angular errors. The average, median, and 95 percentile errors of the 100 test images are evaluated.

Filter type	Pattern	Mapping	Guided filtering	Average	Median	95 percentile
RGB-NIR	Uniform	Linear	No	7.57	4.62	18.25
			Proposed	5.17	3.17	13.36
		Polynomial	No	7.29	4.41	17.67
			Proposed	**4.92**	**2.97**	**11.83**
		Root-polynomial	No	7.73	4.87	18.46
			Proposed	5.35	3.31	13.36
	Hybrid	Linear	No	4.41	3.17	10.49
			Proposed	3.99	**2.92**	9.35
		Polynomial	No	4.06	3.07	9.00
			Proposed	**3.66**	2.94	**7.55**
		Root-polynomial	No	4.35	3.35	9.02
			Proposed	3.91	3.12	7.87
Five band	Miao and Qi	Linear	No	6.63	6.37	10.55
			Proposed	4.74	4.59	7.26
		Polynomial	No	7.00	6.89	10.39
			Proposed	6.48	6.31	9.45
		Root-polynomial	No	5.09	4.79	8.46
			Proposed	**4.02**	**3.74**	**6.43**
	Monno et al.	Linear	No	4.22	4.07	7.08
			Proposed	3.47	3.27	5.84
		Polynomial	No	3.96	3.40	7.72
			Proposed	3.41	2.82	6.56
		Root-polynomial	No	3.32	3.03	6.04
			Proposed	**2.83**	**2.52**	**5.11**

Table 2. Performance evaluation on each illumination. The table shows the average angular errors for the RGB-NIR filter arrays with the polynomial mapping, which is the best performing mapping in Table 1.

Illumination	Uniform RGB-NIR			Hybrid RGB-NIR		
	Standard	Proposed	Improvements	Standard	Proposed	Improvements
Incandescence	16.42	11.51	4.91	7.73	6.54	1.19
Diva light	4.11	2.66	1.45	2.76	2.61	0.15
LED	4.05	2.70	1.35	2.89	2.70	0.19
Fluorescence	3.33	2.11	1.22	1.96	1.97	-0.01
Daylight	8.54	5.62	2.92	4.94	4.47	0.47

our proposed pipeline can also include illumination estimation algorithms [6] or a robust mapping for illumination changes [27] when the illumination condition is unknown.

Parameters of the guided filtering. We used the 5×5 window and the regularization weight 10^{-10} just for avoiding the division by zero in the computation. We selected the G-band image as the guide image for all MSFA types. The following experimental results demonstrate that our proposed pipeline with the guided filtering improves the mapping accuracy, even though the G band is not dominant.

6.2. Experimental Results

Comparison of angular errors. In experiments, we evaluate angular errors, where the angle is defined between the ground-truth and the resultant mapped sRGB vectors in the sRGB space, as an invariant metric for intensity scales of different scenes. We evaluate the average, median, and 95 percentile angular errors of the 100 test images (20 scenes $\times$ 5 illuminations), which are summarized in Table 1. It is shown that our proposed pipeline consistently improves the mapping accuracy for all MSFA types and mapping algorithms. Especially, the 95 percentile errors are much improved. Some of the test images contain severe demosaicking errors because of high-frequency textures or edges, which significantly increases the 95 percentile errors of the standard mapping algorithms. Our proposed pipeline can successfully reduce the amplification and propagation of such demosaicking errors. The polynomial mapping generally offers the best results for the RGB-NIR filter arrays, while the root-polynomial mapping gives the best results for the five-band filter arrays.

Performance evaluation on each illumination. Table 2 shows the average angular errors on each illumination. The table shows the errors for the RGB-NIR filter arrays with the

(a) Input RGB (b) Input NIR (c) Ground-truth sRGB (d) Standard mapping (e) Proposed

Figure 6. Results for the uniform RGB-NIR filter array under the daylight. (a) The input RGB, (b) the input NIR, (c) the target ground-truth sRGB, (d) the standard polynomial mapping, and (e) our proposed pipeline with the polynomial mapping.

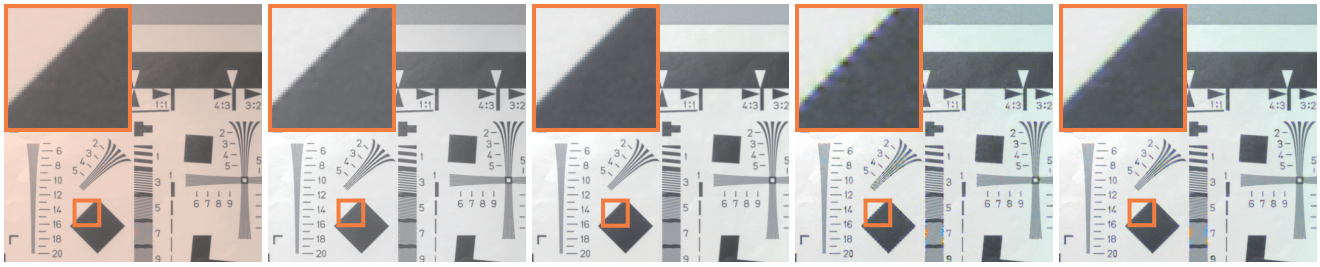

(a) Input RGB (b) Input NIR (c) Ground-truth sRGB (d) Standard mapping (e) Proposed

Figure 7. Results for the for the hybrid RGB-NIR filter array under the incandescence light. (a) The input RGB, (b) the input NIR, (c) the target ground-truth sRGB, (d) the standard polynomial mapping, and (e) our proposed pipeline with the polynomial mapping.

polynomial mapping, which is the best performing mapping in Table 1. For the RGB-NIR filter arrays, our pipeline is especially effective for the incandescent light and the daylight. This is because these two lights have large spectral powers in NIR wavelengths, which requires large mapping coefficients to remove the NIR contaminations of the RGB image. This causes severe error amplification and propagation, which are reduced by the guided filtering.

Visual comparison. Figures 6-9 show the visual comparisons of the mapping results. In Fig. 6 and 7, the NIR band contains relatively large demosaicking errors, which are amplified and propagated by the standard polynomial mapping. In contrast, our pipeline significantly reduces the error amplification and propagation. In Fig. 8 and 9, our pipeline successfully reduces the zipper demosaicking artifacts, which are appeared in the results of the standard root-polynomial mapping.

7. Concluding Remarks

In this paper, we addressed the demosaicking error amplification and propagation in the N-to-sRGB mapping of the single-sensor multispectral imaging. We proposed a novel N-to-sRGB mapping pipeline for reducing the error amplification and propagation by applying the guided filtering in the mapped sRGB space using one of input N band images as the guide image. We experimentally demonstrated that our pipeline consistently improves the mapping accuracy for various MSFA types. Our pipeline is simple and can generally incorporate any existing mapping algorithms. Future works include the investigation of suitable mapping algorithms used with our pipeline, the incorporation of illumination estimation algorithms, and the consideration of noise effects.

Acknowledgment. This work was supported by Strategic Information and Communications R&D Promotion Programme (SCOPE, No.141203024) from Ministry of Internal Affairs and Communications (MIC).

References

[1] B. Bayer. Color imaging array. *U.S. Patent 3971065*, 1976.

[2] J. Brauers and T. Aach. A color filter array based multispectral camera. *12. Workshop Farbbildverarbeitung*, 2006.

[3] Z. Chen, X. Wang, and R. Liang. RGB-NIR multispectral camera. *Optics Express*, 22(5):4985–4994, 2014.

[4] D. Connah, M. S. Drew, and G. D. Finlayson. Spectral edge image fusion: Theory and applications. *Proc. of European Conf. on Computer Vision (ECCV)*, pages 65–80, 2014.

[5] G. D. Finlayson, M. Mackiewiez, and A. Hurlbert. Colour correction using root-polynomial regression. *IEEE Trans. on Image Processing*, 24(5):1460–1470, 2015.

[6] A. Gijsenji, T. Gevers, and J. van de Weijer. Computational color constancy: Survey and experiments. *IEEE Trans. on Image Processing*, 20(9):2475–2489, 2011.

[7] J. Y. Hardeberg, F. Schmitt, and H. Brettel. Multispectral color image capture using a liquid crystal tunable filter. *Optical Engineering*, 41:2532–2548, 2002.

[8] K. He, J. Sun, and X. Tang. Guided image filtering. *IEEE Trans. on Pattern Analysis and Machine Intelligence*, 35(6):1397–1409, 2013.

(a) Input five bands (b) Ground-truth sRGB (c) Standard mapping (d) Proposed

Figure 8. Results for the five-band filter array proposed by Miao and Qi under the LED light. (a) The input five bands, (b) the target ground-truth sRGB, (c) the standard root-polynomial mapping, and (d) our proposed pipeline with the root-polynomial mapping.

(a) Input five bands (b) Ground-truth sRGB (c) Standard mapping (d) Proposed

Figure 9. Results for the five-band filter array proposed by Monno et al. under the fluorescence light. (a) The input five bands, (b) the target ground-truth sRGB, (c) the standard root-polynomial mapping, and (d) our proposed pipeline with the root-polynomial mapping.

[9] G. Hong, M. R. Luo, and P. A. Rhodes. A study of digital camera colorimetric characterisation based on polynomial modelling. *Color Research and Application*, 26(1):76–84, 2001.

[10] P. C. Hung. Colorimetric calibration in electronic imaging devices using a look-up-table model and interpolations. *Journal of Electronic Imaging*, 2(1):53–61, 1993.

[11] H. R. Kang. *Computational color technology*. SPIE Press, 2006.

[12] H. R. Kang and P. G. Anderson. Neural network applications to the color scanner and printer calibrations. *Journal of Electronic Imaging*, 1(2):125–135, 1992.

[13] I. Kharitonenko and W. Li. Image color correction in DCT domain. *Proc. of IEEE Int. Conf. on Consumer Electronics (ICCE)*, pages 245–248, 2013.

[14] D. Kiku, Y. Monno, M. Tanaka, and M. Okutomi. Simultaneous capturing of RGB and additional band images using hybrid color filter array. *Proc. of SPIE*, 9023:90230V–1–9, 2014.

[15] P. J. Lapray, X. Wang, J. B. Thomas, and P. Gouton. Multispectral filter arrays: Recent advances and practical implementation. *Sensors*, 14(11):21626–21659, 2014.

[16] C. Lau, W. Heidrich, and R. Mantiuk. Cluster-based color space optimizations. *Proc. of IEEE Int. Conf. on Computer Vision (ICCV)*, pages 1172–1179, 2011.

[17] Y. M. Lu, C. Fredembach, M. Vetterli, and S. Süsstrunk. Designing color filter arrays for the joint capture of visible and near-infrared images. *Proc. of IEEE Int. Conf. on Image Processing (ICIP)*, pages 3797–3800, 2009.

[18] R. Lukac. *Single-sensor imaging: methods and applications for digital cameras*. CRC Press, 2008.

[19] L. T. Maloney and B. A. Wandell. Color constancy: a method for recovering surface spectral reflectance. *J. Opt. Soc. Am. A*, 3(1):29–33, 1986.

[20] M. Martinello, A. Wajs, S. Quan, H. Lee, C. Lim, T. Woo, W. Lee, S. S. Kim, and D. Lee. Dual aperture photography: Image and depth from a mobile camera. *Proc. of IEEE Int. Conf. on Computational Photography (ICCP)*, 2015.

[21] L. Miao and H. Qi. The design and evaluation of a generic method for generating mosaicked multispectral filter arrays. *IEEE Trans. on Image Processing*, 15(9):2780–2791, 2006.

[22] L. Miao, H. Qi, R. Ramanath, and W. E. Snyder. Binary tree-based generic demosaicking algorithm for multispectral filter arrays. *IEEE Trans. on Image Processing*, 15(11):3550–3558, 2006.

[23] Y. Monno, D. Kiku, S. Kikuchi, M. Tanaka, and M. Okutomi. Multispectral demosaicking with novel guide image generation and residual interpolation. *Proc. of IEEE Int. Conf. on Image Processing (ICIP)*, pages 645–649, 2014.

[24] Y. Monno, S. Kikuchi, M. Tanaka, and M. Okutomi. A practical one-shot multispectral imaging system using a single image sensor. *IEEE Trans. on Image Processing*, 24(10):3048–3059, 2015.

[25] Y. Monno, M. Tanaka, and M. Okutomi. Multispectral demosaicking using adaptive kernel upsampling. *Proc. of IEEE Int. Conf. on Image Processing (ICIP)*, pages 3218–3221, 2011.

[26] Y. Monno, M. Tanaka, and M. Okutomi. Multispectral demosaicking using guided filter. *Proc. of SPIE*, 8299:82990O–1–7, 2012.

[27] R. Nguyen, D. K. prasad, and M. Brown. Raw-to-raw: Mapping between image sensor color responses. *Proc. of IEEE Conf. on Computer Vision and Pattern Recognition (CVPR)*, pages 3398–3405, 2014.

[28] J. Parkkinen, J. Hallikainen, and T. Jaaskelainen. Characteristic spectra of munsell colors. *J. Opt. Soc. Am. A*, 6(2):318–322, 1989.

[29] Z. Sadeghipoor, Y. M. Lu, and S. Süsstrunk. Correlation-based joint acquisition and demosaicing of visible and near-infrared images. *Proc. of IEEE Int. Conf. on Image Processing (ICIP)*, pages 3226–3229, 2011.

[30] H. Tang, X. Zhang, S. Zhuo, F. Chen, K. N. Kutulakos, and L. Shen. High resolution photography with an RGB-infrared camera. *Proc. of IEEE Int. Conf. on Computational Photography (ICCP)*, 2015.

[31] F. Yasuma, T. Mitsunaga, D. Iso, and S. K. Nayar. Generalized assorted pixel camera: postcapture control of resolution, dynamic range, and spectrum. *IEEE Trans. on Image Processing*, 19(9):2241–2253, 2010.